Energy Material Advances
A SCIENCE PARTNER JOURNAL

RESEARCH ARTICLE

Implantation of Solid Electrolyte Interphase Stabilizer within High-Capacity Silicon Electrode Enabling Enhanced Battery Performance

Xiaohong Wang, Chunhao Li, Zihe Chen, and Yongming Sun*

Wuhan National Laboratory for Optoelectronics, Huazhong University of Science and Technology, Wuhan 430074, China.

*Address correspondence to: yongmingsun@hust.edu.cn

The commercial application of high-capacity silicon (Si) anode in lithium-ion batteries is limited by the marked volume expansion and continuous interface side reactions between the active material and the electrolyte. To address the issues, one popular strategy is to induce functional salt additives to the electrolyte, which could help to construct a robust solid electrolyte interphase (SEI) to resist the undesirable parasitic reactions and fast electrode failure. However, there exists the shortness of the dependency in the solubility of the additive salt and the possible homogeneity of the SEI. In light of this, we propose an innovative method of incorporating an SEI stabilization regent, exemplified by lithium difluorooxalate borate (LiDFOB), in the Si anode. This approach facilitates the effective utilization of the functional SEI stabilizer and impressively enhances the presence of inorganic compounds within the SEI. The resultant stable SEI effectively impedes interfacial side reactions, mitigates substantial expansion/contraction, and promotes the transport of Li^+ ions. As a result, the Si electrode incorporated with LiDFOB displays superior long cycle life and enhanced rate capability, indicating the advancement of planting LiDFOB in the electrode in promoting the development of advanced high-energy-density lithium-ion batteries.

Citation: Wang X, Li C, Chen Z, Sun Y. Implantation of Solid Electrolyte Interphase Stabilizer within High-Capacity Silicon Electrode Enabling Enhanced Battery Performance. *Energy Mater. Adv.* 2024;5:Article 0095. https://doi.org/10.34133/energymatadv.0095

Submitted 30 January 2024
Accepted 29 March 2024
Published 8 May 2024

Introduction

There is an escalating demand for lithium-ion batteries with high energy density to cater to a variety of applications, encompassing portable electronics and electric vehicles [1]. A plausible strategy to augment the energy density of lithium-ion batteries is the advancement of high-capacity electrodes by minimizing the mass utilization of active material [2]. Graphite has traditionally been the anode of choice in commercial lithium-ion batteries, offering a respectable capacity (theoretically 372 $mA\cdot h\cdot g^{-1}$) and a low working potential (~ 0.1 V versus Li/Li^+ in average). Silicon has emerged as a promising substitute for graphite, owing to its superior theoretical specific capacity (4,200 $mA\cdot h\cdot g^{-1}$), appropriate potential (approximately 0.4 V versus Li/Li^+), and natural abundance [3,4]. However, the practical implementation of silicon anodes in commercial batteries is hindered by challenges including substantial volume expansion and ongoing interface side reactions between the active material and the electrolyte [5,6]. Numerous studies have been undertaken to enhance silicon-based anodes, encompassing material structural design [7–10], electrolyte engineering [11,12], and electrode structure design [13–16]. A crucial strategy among them to improve the electrochemical performance of Si electrodes involves the establishment of a stable solid electrolyte interphase (SEI) with a high content of inorganic species using electrolyte additive reagents [17–19]. In contrast to the utilization of conventional bulk electrolytes, the predominantly organic SEIs are inherently brittle, prone to fracturing during the charge/discharge cycling, and exhibit relatively low ionic conductivity. Enhancing the proportion of inorganic components within the SEI has been demonstrated to effectively boost electrochemical performance, particularly in terms of rate capability and cycling stability [20]. This strategy of using electrolyte additives in the electrolyte to construct inorganic-rich SEI has, therefore, attracted considerable attention in the scientific community in recent years [21–23]. While the positive effect of many functional salt additives, their utilization and beneficial efficiency hinge on their solubility and physicochemical properties in the electrolyte. Distinct approaches to additive incorporation may also affect interaction with the active material and its utilization ratio, consequently leading to the formation of diverse SEIs. For example, lithium difluorooxalate borate (LiDFOB), a quintessential functional salt additive in the electrolyte, has exhibited the capability to establish a robust SEI enriched with inorganic compounds, which improves the electrochemical cycling stability [24–26]. However, a possible drawback is that functional salt additives dissolved in the electrolyte cannot be often fully consumed, with less than 50% of the additives utilized during the SEI formation [27]. Moreover, some functional additives may exhibit limited solubility in the solvents of the electrolyte, thereby potentially hindering the full manifestation of their effects [18,22,28,29]. Consequently, it is imperative to devise an efficacious strategy to fully harness the potential of these functional salt additives.

In this study, we investigate a novel approach of directly incorporating a functional salt additive into the electrode, as opposed to dissolving it in the electrolyte. This method substantially enhances its utilization efficiency, constructs a uniform and robust LiF-rich SEI, and subsequently improves the overall electrochemical performance, as exemplified by our use of LiDFOB. Specifically, the decomposition of $DFOB^-$ anions into inorganic species within the SEI is amplified, without necessitating an increase in LiDFOB dosage or incurring additional electrolyte costs (Fig. 1). This stands in contrast to the conventional approach of dissolving LiDFOB salt in the electrolyte, as the proposed method facilitates a more extensive reduction of $DFOB^-$ anions. Moreover, the efficacy of our functional electrode stabilizer was systematically validated through a variety of characterizations. These induce the formation of a stable SEI, thereby obstructing interfacial side reactions, impeding the formation of crystalline $Li_{15}Si_4$ (c-$Li_{15}Si_4$), and mitigating significant expansion/contraction during the charge/discharge cycles. This approach delineates a promising strategy for enhancing the efficiency of functional reagents, while concurrently mitigating the associated costs and potential adverse effects that may arise from the introduction of high-content additives.

Materials and Methods

Electrode preparation

Si powder used in this investigation was sourced from photovoltaic waste and was used as the anode active material without further treatments. A uniform slurry was subsequently prepared by incorporating Si, carbon black, and polyacrylic acid in a weight ratio of 8:1:1 into *N*-methylpyrrolidone. Subsequently, the slurry was cast on a copper foil, subjected to a drying process at 80 °C for a duration of 12 h under vacuum conditions, and followed by calendaring. The resultant electrode was then cut into discs with a diameter of 10 mm. The aforementioned procedures were meticulously repeated to prepare Si-2DFOB, Si-5DFOB, and Si-DFOB, with the only variation being the incorporation of 2, 5, and 10 wt% of LiDFOB into the Si powder, respectively. Si electrodes with LiDFOB necessitate no special treatments or preservation during the experiment due to its good environmental stability. The typical mass loading of the electrode in our study was ~ 1 $mg\cdot cm^{-2}$. The cells for measurements were assembled in a glove box filled with argon (H_2O, $O_2 <$ 1 ppm). During the cell assembly, lithium foils were used as the counter electrodes, and a polypropylene film was functioned as the separator. The electrolyte was composed of 1 M $LiPF_6$ with (or without) 0.1 M LiDFOB in a solvent mixture of ethylene carbonate (EC), ethyl methyl carbonate (EMC), diethyl carbonate (DEC), and fluoroethylene carbonate (FEC) (3:3:3:1 vol%). It should be noted that the electrolyte utilized in the battery with the Si-DFOB electrode did not contain LiDFOB and the electrolyte for Si electrode contained 0.1 M LiDFOB.

Electrochemical characterizations

The long-term electrochemical cycling tests were conducted using Land battery testers (Wuhan Land Electronic Co. Ltd., China) at a rate of 1 C (1 C = 2,000 $mA\cdot h\cdot g^{-1}$) within the voltage range of 0.01 to 1.0 V (versus Li/Li^+). Cyclic voltammetry (CV) and electrochemical impedance spectroscopy (EIS) measurements were carried out on a biologic electrochemical workstation. The scanning speed ranged from 0.01 to 0.1 $mV\cdot s^{-1}$ within the potential window of 0.01 to 1.0 V (versus Li/Li^+). EIS curves were obtained over a frequency range of 10 mHz to 100 kHz with an amplitude of 10 mV.

Physical characterizations

To characterize the phase information of Si, an x-ray diffraction pattern was performed using a PANalytical B. V. instrument (Cu Kα). Morphological characteristics of materials and electrodes were depicted through scanning electron microscopy (SEM; Nova NanoSEM 450) and high-resolution transmission electron microscopy (HR-TEM; Talos F200X). The electrodes were cycled in the electrolyte without FEC to avoid its influence on the result. X-ray photoelectron spectroscopy (XPS) measurements (Thermo Fisher Scientific ESCALAB 250Xi, USA) were operated to trace the interphase composition and chemical states. Before tests, all the electrodes were washed repeatedly with dimethyl carbonate.

Results and Discussion

Si particles, characterized by an irregular morphology and sizes ranging from 200 nm to 1.5 μm, exhibit a pure phase structure (JCPDS 77-2110) devoid of impurities (Fig. S1). A marginal improvement in cycling performance and a notable optimization in rate capability are observed when the LiDFOB amount is increased from 2 to 10 wt% (Fig. S2). Si-DFOB (10 wt% of LiDFOB) has been selected for further investigation. Within the Si-DFOB electrode, the concentration of LiDFOB, once fully dissolved in the electrolyte, is approximately 0.007 M, a value

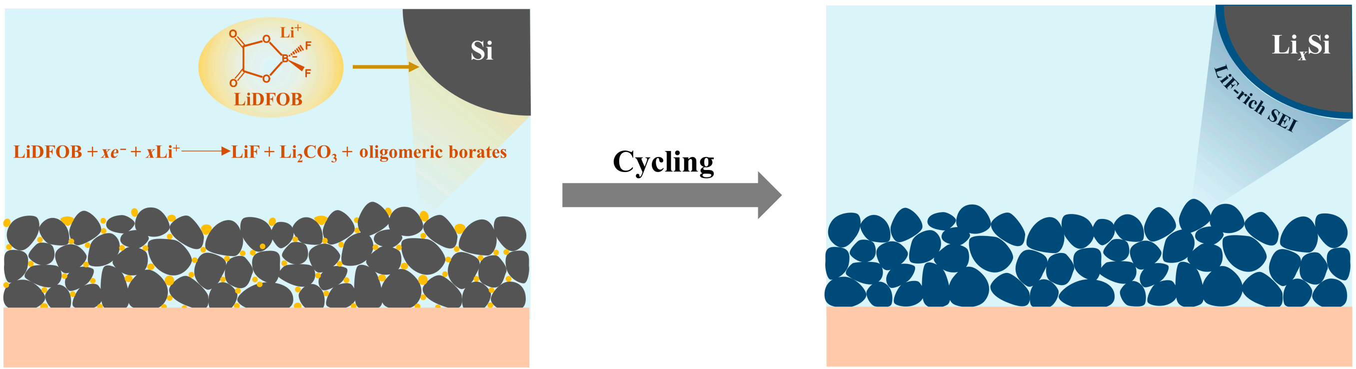

Fig. 1. Schematic illustration of the embedment of the functional LiDFOB salt in the electrode for stabilizing Si-based anode.

markedly lower than 0.1 M observed in other studies by directly dissolving LiDFOB into the electrolyte before its use [25,26]. The Si and Si-DFOB electrodes demonstrate reversible capacities of 2,609.9 and 2,665.6 mA·h·g^{-1} for the first charge/discharge cycle, respectively, with initial coulombic efficiencies (ICEs) of 77.9% and 81.6% (Fig. 2A and B). Remarkably, after 100 cycles at 1 C, the Si-DFOB electrode delivers a capacity of 1,392.2 mA·h·g^{-1} (1.33 mA·h·cm^{-2}), surpassing 976.4 mA·h·g^{-1} (1.0 mA·h·cm^{-2}) achieved by the Si electrode (Fig. S3). The mid-voltage difference (ΔV) during charge and discharge processes for Si-DFOB is lower than that of Si (0.28 and 0.31 V after 100 cycles, respectively), indicating reduced polarization (Fig. 2C). Concurrently, while Si exhibits minimal capacity at 5 C, Si-DFOB retains 361.6 mA·h·g^{-1} at the same current density (Fig. 2D and Fig. S4). Si-DFOB demonstrates a considerable performance compared to many reported Si-based materials/electrodes (Table S1). The high ICE, stable cycle performance, and enhanced rate capability of the Si-DFOB electrode can be ascribed to the uniform distribution and effective decomposition of LiDFOB and the formation of a robust SEI on the Si surface.

The chemical characteristics of SEIs of electrodes were elucidated using XPS (Fig. 3). The C 1s peaks correspond to C–C (284.8 eV), C–O (286.6 eV), C═O (288.3 eV), and Li_2CO_3 (~290 eV), while the O 1s peaks are attributed to Li_2O (528.5 eV), C═O (531.6 eV), and C–O (533.6 eV) (Fig. 3B and C), respectively, signifying the decomposition products of the electrolyte [30–33]. Moreover, the high-resolution F 1s spectrum exhibits a distinct peak at 684.7 eV, indicative of LiF, with a higher prevalence observed on the Si-DFOB surface based on atomic percentage (Fig. 3A and D) [17,30,32]. The presence of B–O (190.8 eV) and B–F (193.2 eV) peaks in the B 1s spectrum confirms the reduction of DFOB$^-$ (Fig. 3E) [34,35]. The comparable B atomic ratios on both Si and Si-DFOB surfaces suggest a similar contribution of DFOB$^-$ anions from the electrolyte and the electrode to the SEI formation, despite the low concentration of LiDFOB in the electrode. Consequently, the integration of LiDFOB into the electrode enhances its utilization efficiency. The uniform distribution and effective reduction of LiDFOB in the Si electrode contribute to the formation of a thin and homogeneous SEI rich in inorganic compounds [21,25,34]. This result

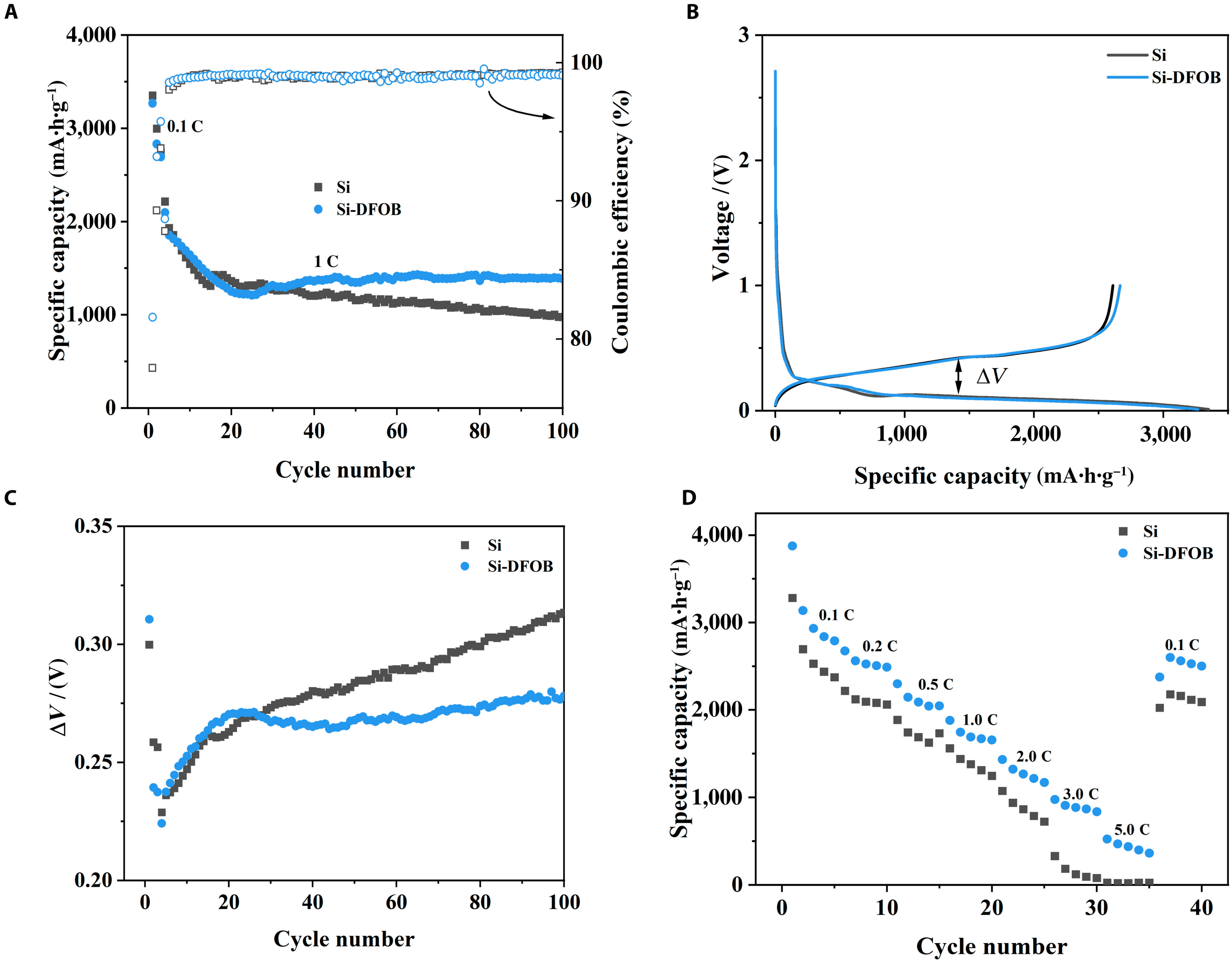

Fig. 2. Electrochemical charge/discharge performance of Si and Si-DFOB electrodes. (A) Electrochemical cycling performance of the 2 electrodes at 1 C after 3 cycles at 0.1 C between 0.01 and 1.0 V. (B) Galvanostatic voltage curves of the first cycle at 0.1 C. (C) Difference between charge and discharge mid-voltage for different cycles. (D) Rate capability from 0.1 to 5.0 C.

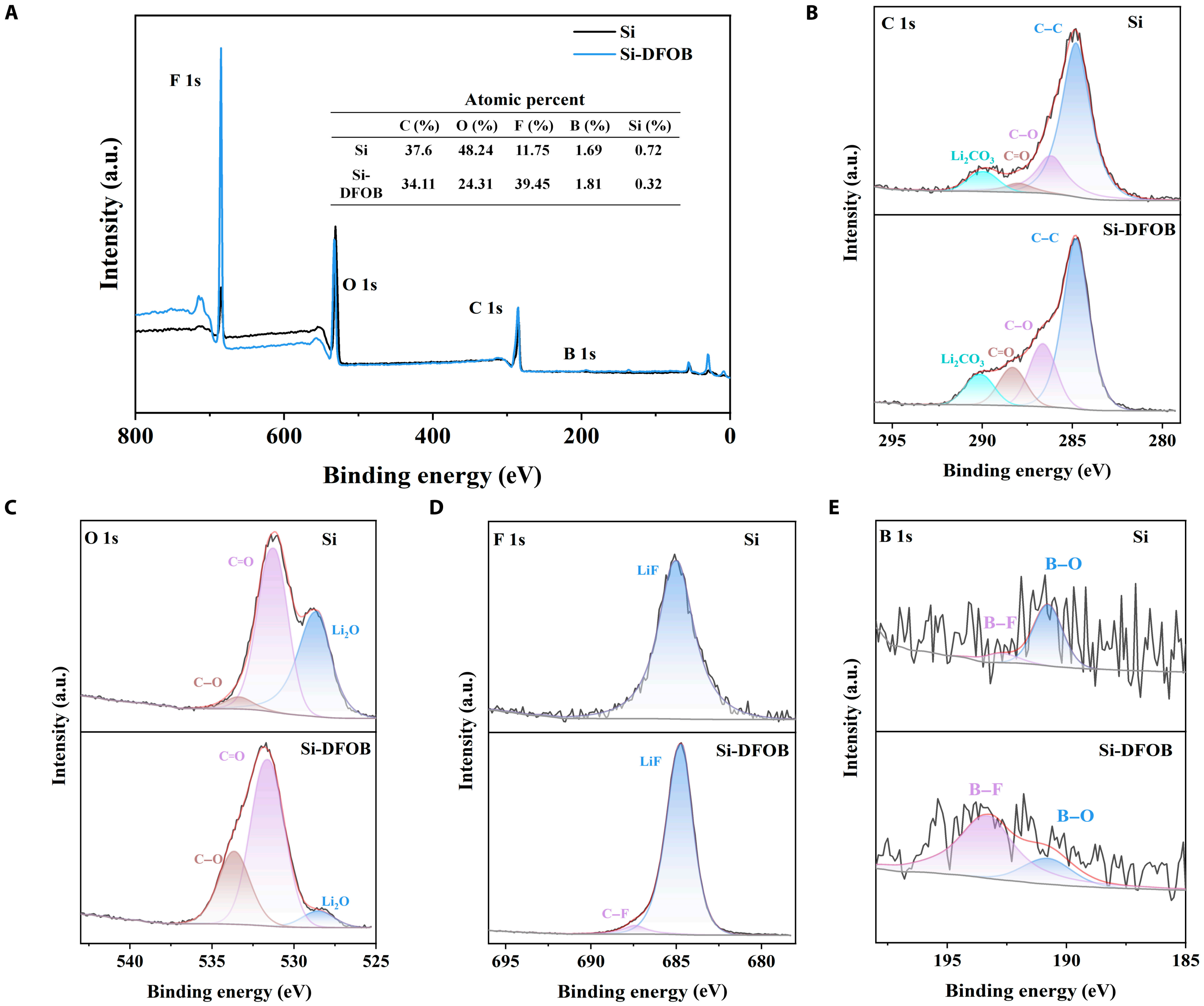

Atomic percent

	C (%)	O (%)	F (%)	B (%)	Si (%)
Si	37.6	48.24	11.75	1.69	0.72
Si-DFOB	34.11	24.31	39.45	1.81	0.32

Fig. 3. Surface characteristics of Si and Si-DFOB electrodes after 100 cycles. (A) Survey scan, high-resolution (B) C 1s, (B) O 1s, (C) F 1s, and (D) B 1s XPS spectra. a.u., arbitrary units.

is also verified by HR-TEM investigation (Fig. S5). The composition facilitates the movement of Li^+ ions and enhances the rate performance. In summary, these findings suggest that the incorporation and effective reduction of LiDFOB in the Si electrode play a pivotal role in the formation of a conductive SEI for improved electrochemical performance.

Upon the integration of LiDFOB into the electrode, the decomposition of $DFOB^-$ transpires not only on the surface but also intrinsically. A novel insight reveals that the presence of FEC facilitates the introduction of LiF into the bulk phase, thereby mitigating the formation of c-$Li_{15}Si_4$, reducing the volume effect, and alleviating Li-trapping [36]. The synergistic effect of $DFOB^-$ and FEC results in an increased content of LiF in the bulk. LiDFOB, when incorporated into the electrode, may exhibit a superior ability in mitigating the volume effect compared to when it is merely dissolved in the electrolyte. The pristine Si and Si-DFOB electrodes depicted in Fig. 4A and C reveal no substantial difference between them, suggesting the negligible effect of LiDFOB on the primary morphology. The top-view SEM images demonstrate that the surface of the cycled Si-DFOB electrode remains largely intact (Fig. 4D), while the surface of the cycled Si electrode is noticeably damaged (Fig. 4B). The cross-sectional SEM images of both the Si electrode and Si-DFOB electrode before and after 100 cycles, as illustrated in Fig. 4E to H, indicate that the thickness of the Si-DFOB anode ranges from 8 to 15.8 μm, with a lower volume change rate. Therefore, the integration of LiDFOB into the electrode effectively diminishes the expansion and maintains interface stability. In addition, the EIS test was used to evaluate the transport of Li^+ ions within the SEI (Fig. 4I to K). Prior to cycling, the SEI resistance (R_{SEI}) of the Si-DFOB electrode surpasses that of the Si electrode (Fig. S6). R_{SEI} of Si-DFOB is 26.3 Ω after 5 cycles and 32.3 Ω after 50 cycles, which is lower than that of the Si anode (30.3 Ω after 5 cycles and 38.8 Ω after 50 cycles). This suggests that the homogeneous SEI of the Si-DFOB, rich in inorganic compounds, can reduce the interface resistance and promote the migration of Li^+ ions.

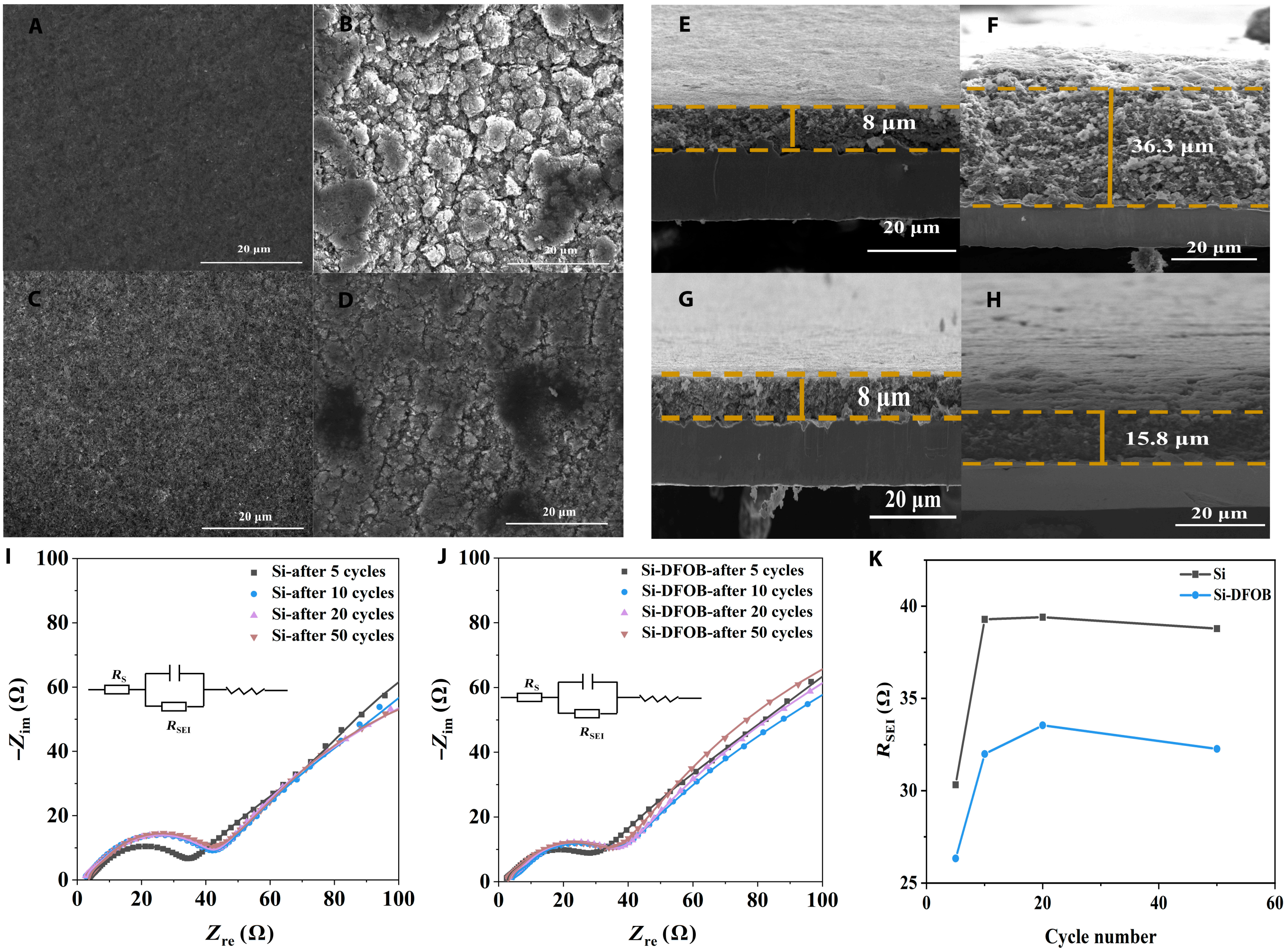

Fig. 4. Variations in thickness and R_{SEI} of Si and Si-DFOB electrodes. Top-view SEM images of pristine (A) Si and (C) Si-DFOB electrodes. Top-view SEM images of (B) Si and (D) Si-DFOB electrodes after 100 cycles. Cross-sectional SEM images of pristine (E) Si and (G) Si-DFOB electrodes. Cross-sectional SEM images of (F) Si and (H) Si-DFOB electrodes after 100 cycles. Nyquist plots of (I) Si and (J) Si-DFOB electrodes after 5, 10, 20, and 50 cycles. (K) Variation of R_{SEI} during cycling.

To investigate the diffusion of Li^+ ions within the bulk phase, we used CV tests to evaluate the kinetic performance (Fig. 5). The peaks at 1.6 and 1.1 V are attributed to the decomposition of LiDFOB and FEC, respectively (Fig. S7) [37–39]. The reduction peaks at 0.05 and 0.2 V, denoted as i_{pa1} and i_{pa2}, correspond to the lithiation of the Si anode. The oxidation peaks at 0.3 and 0.45 V, denoted as i_{pc1} and i_{pc2}, are associated with the dealloying process (Fig. 5A) [8,40,41]. It is observed that i_{pa1}, i_{pa2}, and i_{pc1} are linearly correlated with $v^{1/2}$ (Fig. 5C). The apparent diffusion coefficient (D) can be calculated using the equation $i_p = 2.69 \times 10^5 A n^{3/2} C_0 D^{1/2} v^{1/2}$ [42–44], where A, n, and C_0 represent the geometric area of electrodes, the charge transfer number, and the concentration of Li^+ ions, respectively. The results suggest that the diffusion of Li^+ ions in the Si-DFOB anode is rapid (Table). However, i_{pc2} (~0.45 V), associated with the dealloying of c-$Li_{15}Si_4$, is not linearly correlated with $v^{1/2}$ (Fig. 5C) [36,45,46]. As the scanning rate increases, the lithiation capacity decreases, and less c-$Li_{15}Si_4$ is formed. The percentage of i_{pc2} in the sum of i_{pc1} and i_{pc2} can be used to roughly estimate the proportion of c-$Li_{15}Si_4$ (Fig. 5D). Despite the Si-DFOB electrode delivering more capacity, the ratio of c-$Li_{15}Si_4$ decreases, attributable to the homogeneity of the alloying reaction and the suppression of the formation of c-$Li_{15}Si_4$. This result aligns with the dQ/dV (Fig. 5E and F). The decomposition products of LiDFOB incorporated into the Si electrode inhibit the formation of c-$Li_{15}Si_4$, alleviate expansion, and enhance the diffusion of Li^+ ions [36,45–48].

Table. D of Li^+ ions in Si and Si-DFOB

	D_{pa1} (cm^2·s^{-1})	D_{pa2} (cm^2·s^{-1})	D_{pc1} (cm^2·s^{-1})
Si	1.87×10^{-11}	4.23×10^{-12}	2.88×10^{-12}
Si-DFOB	2.80×10^{-11}	1.06×10^{-11}	5.53×10^{-11}

Conclusion

We adopted a strategy of incorporating LiDFOB into the Si electrode to ensure its efficient reduction and enhancement in electrochemical performances. This methodology is distinguished by its simplicity, cost-effectiveness, and ease of integration with

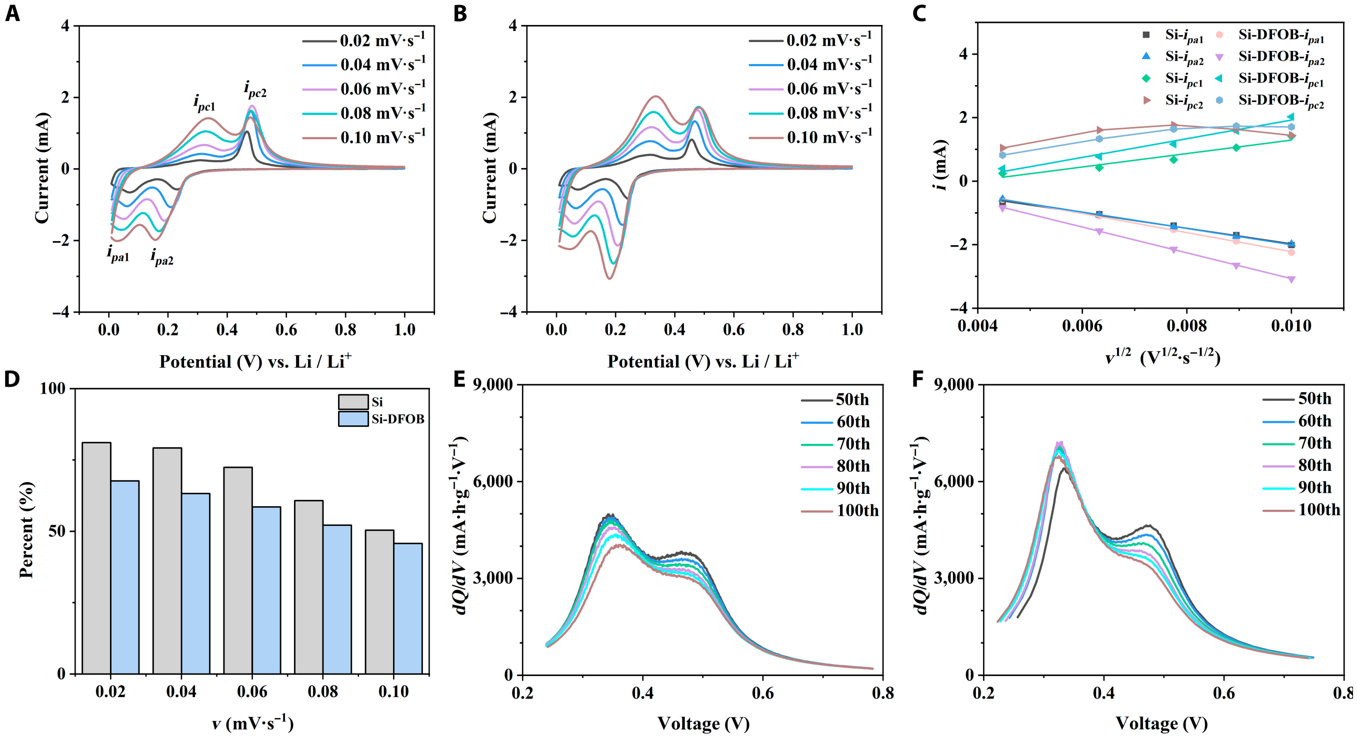

Fig. 5. Kinetic performance of Si and Si-DFOB electrodes. CV tests of (A) Si and (B) Si-DFOB electrodes at 0.02, 0.04, 0.06, 0.08, and 0.1 mV·s^{-1}. (C) Relationship of i_p and $v^{1/2}$. (D) Percentage of i_{pc2} in i_{pc2} and i_{pc1} at varied scan rates. dQ/dV curves of (E) Si and (F) Si-DFOB electrodes at different cycles.

existing electrode production processes. The utilization rate of LiDFOB, when incorporated into the electrode, exceeds that of LiDFOB when directly dissolved in the electrolyte. The complete reduction of LiDFOB results in the formation of a uniform and durable SEI, which mitigates continuous side reactions, alleviates expansion, and enhances the diffusion of Li$^+$ ions. Consequently, Si-DFOB exhibits a high ICE, low polarization, stable cycling performance, and enhanced rate capability.

Acknowledgments

We would like to thank the Analytical and Testing Center of Huazhong University of Science and Technology for providing facilities.

Funding: This work is supported by the Natural Science Foundation of China (no. 52072137).

Author contributions: X. W. performed conceptualization, methodology, data curation, and writing the draft. C. L. conducted the SEM tests. Z. C. was responsible for the schematic drawing. Y. S. performed supervision, conceptualization, writing-review and editing. All authors discussed and contributed to the final manuscript.

Competing interests: The authors declare that they have no competing interests.

Data Availability

The online version contains supplementary materials available free of charge.

Supplementary Materials

Figs. S1 to S7
Table S1

References

1. Ge M, Cao C, Biesold GM, Sewell CD, Hao S-M, Huang J, Zhang W, Lai Y, Lin Z. Recent advances in silicon-based electrodes: From fundamental research toward practical applications. *Adv Mater*. 2021;33(16):2004577.
2. Li Y, Li Q, Chai J, Wang Y, Du J, Chen Z, Rui Y, Jiang L, Tang B. Si-based anode lithium-ion batteries: A comprehensive review of recent progress. *ACS Mater Lett*. 2023;5(11):2948–2970.
3. Sun L, Liu Y, Wu J, Shao R, Jiang R, Tie Z, Jin Z. A review on recent advances for boosting initial coulombic efficiency of silicon anodic lithium ion batteries. *Small*. 2022;18(5):2102894.
4. Song A, Zhang W, Guo H, Dong L, Jin T, Shen C, Xie K. A review on the features and progress of silicon anodes-based solid-state batteries. *Adv Energy Mater*. 2023;13(39):2301464.
5. Yang D, Ng YXA, Zhang K, Chang Q, Chen J, Liang T, Cheng S, Sun Y, Shen W, Ang EH, et al. Imaging the surface/interface morphologies evolution of silicon anodes using in situ/operando electron microscopy. *ACS Appl Mater Interfaces*. 2023;15(17):20583–20602.
6. Zhu B, Wang X, Yao P, Li J, Zhu J. Towards high energy density lithium battery anodes: Silicon and lithium. *Chem Sci*. 2019;10(30):7132–7148.
7. Han X, Gu L, Sun Z, Chen M, Zhang Y, Luo L, Xu M, Chen S, Liu H, Wan J, et al. Manipulating charge-transfer kinetics and a flow-domain LiF-rich interphase to enable high-performance microsized silicon-silver-carbon composite anodes for solid-state batteries. *Energy Environ Sci*. 2023;16(11):5395–5408.
8. Yang Z, Wu C, Li S, Qiu L, Yang Z, Zhong Y, Zhong B, Song Y, Wang G, Liu Y, et al. A unique structure of highly stable interphase and self-consistent stress distribution radial-gradient porous for silicon anode. *Adv Funct Mater*. 2022;32(13):2107897.

9. Lee T, Kim N, Lee J, Lee Y, Sung J, Kim H, Chae S, Cha H, Son Y, Kwak SK, et al. Suppressing deformation of silicon anodes via interfacial synthesis for fast-charging lithium-ion batteries. *Adv Energy Mater*. 2023;13(41):2301139.
10. Chae S, Kwak W-J, Han KS, Li S, Engelhard MH, Hu J, Wang C, Li X, Zhang J-G. Rational design of electrolytes for long-term cycling of Si anodes over a wide temperature range. *ACS Energy Lett*. 2021;6(2):387–394.
11. Yeom SJ, Wi T-U, Jung S-J, Kim MS, Jeon S-C, Lee H-W. Near zero-strain silicon oxycarbide interphases for stable Li-ion batteries. *Chem Comm*. 2023;59(80):11963–11966.
12. Ghaur A, Peschel C, Dienwiebel I, Haneke L, Du L, Profanter L, Gomez-Martin A, Winter M, Nowak S, Placke T. Effective SEI formation via phosphazene-based electrolyte additives for stabilizing silicon-based lithium-ion batteries. *Adv Energy Mater*. 2023;13(26):2203503.
13. Mu T, Xiang L, Wan X, Lou S, Du C, Zuo P, Yin G. Ultrahigh areal capacity silicon anodes realized via manipulating electrode structure. *Energy Storage Mater*. 2022;53:958–968.
14. Yang Y, Wang J, Kim SC, Zhang W, Peng Y, Zhang P, Vilá RA, Ma Y, Jeong YK, Cui Y. In situ prelithiation by direct integration of lithium mesh into battery cells. *Nano Lett*. 2023;23(11):5042–5047.
15. Ko S, Baek M-J, Wi T-U, Kim J, Park C, Lim D, Yeom SJ, Bayramova K, Lim HY, Kwak SK, et al. Understanding the role of a water-soluble catechol-functionalized binder for silicon anodes by diverse in situ analyses. *ACS Mater Lett*. 2022;4(5):831–839.
16. Yeom SJ, Wi T-U, Ko S, Park C, Bayramova K, Jin S, Lee SW, Lee H-W. Nitrogen plasma-assisted functionalization of silicon/graphite anodes to enable fast kinetics. *ACS Appl Mater Interfaces*. 2022;14(4):5237–5246.
17. Tian M, Jin Z, Song Z, Qiao R, Yan Y, Yu H, Ben L, Armand M, Zhang H, Zhou Z, et al. Domino reactions enabling sulfur-mediated gradient interphases for high-energy lithium batteries. *J Am Chem Soc*. 2023;145(39):21600–21611.
18. Gupta A, Yang Z, Trask S, Bloom I, Johnson C. The electrochemical stabilization of silicon anodes via a locally concentrated $LiNO_3$ complex. *J Electrochem Soc*. 2023;170(1):Article 010504.
19. Kim K, Ma H, Park S, Choi N-S. Electrolyte-additive-driven interfacial engineering for high-capacity electrodes in lithium-ion batteries: Promise and challenges. *ACS Energy Lett*. 2020;5(5):1537–1553.
20. Wan H, Xu J, Wang C. Designing electrolytes and interphases for high-energy lithium batteries. *Nat Rev Chem*. 2024;8:30–44.
21. Cao Z, Zheng X, Qu Q, Huang Y, Zheng H. Electrolyte design enabling a high-safety and high-performance Si anode with a tailored electrode-electrolyte interphase. *Adv Mater*. 2021;33(38):2103178.
22. Liu S, Ji X, Piao N, Chen J, Eidson N, Xu J, Wang P, Chen L, Zhang J, Deng T, et al. An inorganic-rich solid electrolyte interphase for advanced lithium-metal batteries in carbonate electrolytes. *Angew Chem Int Ed*. 2021;60(7):3661–3671.
23. Mao M, Ji X, Wang Q, Lin Z, Li M, Liu T, Wang C, Hu Y-S, Li H, Huang X, et al. Anion-enrichment interface enables high-voltage anode-free lithium metal batteries. *Nat Commun*. 2023;14(1):1082.
24. Jamal A, Salian GD, Mathew A, Wahyudi W, Carvalho RP, Gond R, Heiskanen SK, Brandell D, Younesi R. Tris(trimethylsilyl) phosphite and lithium difluoro(oxalato) borate as electrolyte additives for $LiNi_{0.5}Mn_{1.5}O_4$-graphite lithium-ion batteries. *ChemElectroChem*. 2023;10(16):Article e202300139.
25. Huang S, Wang S, Hu G, Cheong L-Z, Shen C. Modulation of solid electrolyte interphase of lithium-ion batteries by LiDFOB and LiBOB electrolyte additives. *App Sur Sci*. 2018;441: 265–271.
26. Wang C, Liu S, Xu H, Wang X, Tian G, Fan F, Liu P, Wang S, Zeng C, Shu C. Adjusting Li^+ solvation structures via dipole-dipole interaction to construct inorganic-rich interphase for high-performance Li metal batteries. *Small*. 2024;2024:2308995.
27. Han Y, Xu J, Wang W, Long F, Qu Q, Wang Y, Zheng H. Implanting an electrolyte additive on a single crystal Ni-rich cathode surface for improved cycleability and safety. *J Mater Chem A*. 2020;8(46):24579–24589.
28. Liu S, Xia J, Zhang W, Wan H, Zhang J, Xu J, Rao J, Deng T, Hou S, Nan B, et al. Salt-in-salt reinforced carbonate electrolyte for Li metal batteries. *Angew Chem Int Ed*. 2022;134(43):Article e202210522.
29. Yang H, Chen X, Yao N, Piao N, Wang Z, He K, Cheng H-M, Li F. Dissolution-precipitation dynamics in ester electrolyte for high-stability lithium metal batteries. *ACS Energy Lett*. 2021;6(4):1413–1421.
30. Liu Z, Ma S, Mu X, Li R, Yin G, Zuo P. A scalable cathode chemical prelithiation strategy for advanced silicon-based lithium ion full batteries. *ACS Appl Mater Interfaces*. 2021;13(10):11985–11994.
31. Zhang Y, Wang W-P, Zhao Y, Zhang X, Guo H, Gao H, Xu D-X, Zhao Y-M, Li G, Liang J-Y, et al. Exacerbated high-temperature calendar aging of SiO_x-graphite electrode induced by interparticle lithium crosstalk. *Adv Funct Mater*. 2024;34(2):2310309.
32. Yang Y, Yang Z, Li Z, Wang J, He X, Zhao H. Rational electrolyte design for interfacial chemistry modulation to enable long-term cycling Si anode. *Adv Energy Mater*. 2023;13(41):2302068.
33. Jiao S, Ren X, Cao R, Engelhard MH, Liu Y, Hu D, Mei D, Zheng J, Zhao W, Li Q, et al. Stable cycling of high-voltage lithium metal batteries in ether electrolytes. *Nat Energy*. 2018;3(9):739–746.
34. Zhang K, Tian Y, Wei C, An Y, Feng J. Building stable solid electrolyte interphases (SEI) for microsized silicon anode and 5V-class cathode with salt engineered nonflammable phosphate-based lithium-ion battery electrolyte. *Appl Surf Sci*. 2021;553:Article 149566.
35. Lv L, Wang Y, Huan W, Wang Y, Zhu G, Zheng H. Effect of lithium salt type on silicon anode for lithium-ion batteries. *Electrochim Acta*. 2022;413:Article 140159.
36. Li Y, Cao Z, Wang Y, Lv L, Sun J, Xiong W, Qu Q, Zheng H. New insight into the role of fluoro-ethylene carbonate in suppressing Li-trapping for Si anodes in lithium-ion batteries. *ACS Energy Lett*. 2023;8(10):4193–4203.
37. Rynearson L, Jayawardana C, Yeddala M, Lucht BL. Improved performance of silicon-containing anodes with organic solvent-solubilized lithium nitrate. *J Electrochem Soc*. 2023;170(6):Article 060525.
38. Li B, Shao Y, He J, Chen R, Huang S, Wu Z, Li J, Wang Z, Liu G. Cyclability improvement of high voltage lithium cobalt oxide/graphite battery by use of lithium difluoro(oxalate)borate electrolyte additive. *Electrochim Acta*. 2022;426:Article 140783.
39. Jin Y, Kneusels N-JH, Magusin PCMM, Kim G, Castillo-Martínez E, Marbella LE, Kerber RN, Howe DJ,

Paul S, Liu T, et al. Identifying the structural basis for the increased stability of the solid electrolyte interphase formed on silicon with the additive fluoroethylene carbonate. *J Am Chem Soc*. 2017;139(42):14992–15004.

40. Yeom SJ, Lee C, Kang S, Wi T-U, Chanhee L, Chae S, Cho J, Shin DO, Ryu J, Lee H-W. Native void space for maximum volumetric capacity in silicon-based anodes. *Nano Lett*. 2019;19(12):8793–8800.
41. Zhang J, Wang D, Yuan R, Li X, Li J, Jiang Z, Li A, Chen X, Song H. Simple construction of multistage stable silicon-graphite hybrid granules for lithium-ion batteries. *Small*. 2023;19(17):2207167.
42. Tao X, Wang J, Liu C, Wang H, Yao H, Zheng G, Seh ZW, Cai Q, Li W, Zhou G, et al. Balancing surface adsorption and diffusion of lithium-polysulfides on nonconductive oxides for lithium-sulfur battery design. *Nat Commun*. 2016;7(1):11203.
43. Wang J, KoenigJr GM. Comparison of lithium diffusion coefficient measurements in tellurium electrodes via different electrochemical techniques. *J Electrochem Soc*. 2023;170(5):Article 050534.
44. Zhan R, Liu S, Wang W, Chen Z, Tu S, Wang X, Ge H, Luo H, Chai T, Ou Y, et al. Micrometer-scale single crystalline particles of niobium titanium oxide enabling an Ah-level pouch cell with superior fast-charging capability. *Mater Horiz*. 2023;10(11):5246–5255.
45. Obrovac MN, Krause LJ. Reversible cycling of crystalline silicon powder. *J Electrochem Soc*. 2007;154(2):A103–A108.
46. Chevrier VL, Liu L, Le DB, Lund J, Molla B, Reimer K, Krause LJ, Jensen LD, Figgemeier E, Eberman KW. Evaluating Si-based materials for Li-ion batteries in commercially relevant negative electrodes. *J Electrochem Soc*. 2014;161(5):A783–A791.
47. Fu F, Wang X, Zhang L, Yang Y, Chen J, Xu B, Ouyang C, Xu S, Dai F-Z, E W. Unraveling the atomic-scale mechanism of phase transformations and structural evolutions during (de) lithiation in Si anodes. *Adv Funct Mater*. 2023;33(37):2303936.
48. Gan C, Ye X, Zhang S, Chen J, Wen W, Liu Y, Peng D-L, Tang L, Luo X. Current density induced growth of $Li_{15}Si_4$ alloy in silicon-carbon anodes during first lithiation process. *J Energy Storage*. 2021;41:Article 102930.